Improving the Long-Term Stability of Perovskite Solar Cells with a Porous Al_2O_3 Buffer-Layer

Simone Guarnera[1,2,3], Antonio Abate[3*†], Wei Zhang[3], Jamie M. Foster[4†], Giles Richardson[4], Annamaria Petrozza[1*], Henry J. Snaith[3*]

[1] Center for Nano Science and Technology@PoliMi, Istituto Italiano di Tecnologia, Via Pascoli 70/3, 20133 Milano, Italy

[2] Dipartimento di Fisica, Politecnico di Milano, Piazza L. da Vinci 32, 20133 Milano, Italy

[3] Clarendon Laboratory, Department of Physics, University of Oxford, Parks Road, Oxford, OX1 3PU, United Kingdom

[4] School of Mathematics, University of Southampton, Southampton, Hampshire, SO17 1BJ, United Kingdom

[†] present address: JMF: School of Mathematics and Statistics, McMaster University, Hamilton, Ontario, L8S 4L8, Canada. AA: Laboratory of Photonics and Interfaces, Department of Chemistry and Chemical Engineering, Swiss Federal Institute of Technology, Station 6, CH-1015 Lausanne, Switzerland

***Corresponding authors:** AA a.abate@epfl.ch, AP annamaria.petrozza@iit.it, HJS h.snaith1@physics.ox.ac.uk

Abstract

Hybrid perovskites represent a new paradigm for photovoltaics, which have the potential to overcome the performance limits of current technologies and achieve low cost and high versatility. However, an efficiency drop is often observed within the first few hundred hours of device operation, which could become an important issue. Here we demonstrate that the electrode's metal migrating through the hole transporting material (HTM) layer and eventually contacting the perovskite is in part responsible for this early device degradation. We show that depositing the HTM within an insulating mesoporous "buffer layer" comprising of Al_2O_3 nanoparticles, prevents the metal electrode migration while allowing for precise control of the HTM thickness. This enables an improvement in the solar cell fill factor and prevents degradation of the device after 350 hours of operation.

TOC graphic

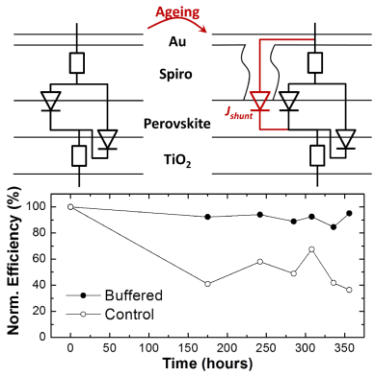

Keywords: perovskite solar cells, stability, buffer layer, electric shunting pathway, photovoltaic, ageing test.

The global energy demand has grown significantly over the last decades and it is predicted to keep growing in the next years [1–3]. To compensate this trend, the production from fossil fuels will be increasingly backed up by energy from renewable sources. In particular, the contribution from solar energy is expected to play a significant role in the near future.

So far, dye-sensitized solar cells (DSSCs) have been one of the most promising technologies to deliver cost-effective solar power which have been intensively investigated over the last 20 years [4–9]. Emerging from the field of DSSCs, the inorganic-organic perovskite materials have been used to fabricate high-performance hybrid solar cells within the last two years, with power conversion efficiencies (PCE) up to 20% [10]. Such performances are quite striking considering the extremely young technology. In the first demonstration, Kojima and co-workers used methylammonium lead halides ($CH_3NH_3PbX_3$) as TiO_2 sensitizer in a device architecture identical to a DSSC, which has been described as perovskite-sensitized solar cell (PSSC) [11]. A few years later, Lee and co-workers demonstrated that $CH_3NH_3PbX_3$, prepared from a particular precursors solution with a source of both iodine and chlorine, can effectively support charge transport as well as being a good light absorber [12]. This enabled the development of a new device configuration, named meso-superstructured solar cell (MSSC). In MSSCs an insulating mesoporous Al_2O_3 layer substitutes the mesoporous TiO_2 and acts simply as a scaffold for the perovskite rather than as an electron transporter. These development have enabled perovskite solar cells to emerge as a new technology in their own right, with all the most efficient devices incorporating a solid thin-film absorber layer which absorbs light, generates free carriers and transports those carriers to the contacts. The efficiency of devices based on this simple architecture can be further improved passivating the perovskite surface [13]. Regardless the particular device architecture, incorporating mesoporous scaffolds or planar contacts, perovskite-based solar cells have been demonstrated

at lab scale to be competitive with the best established photovoltaic technologies in terms of power conversion efficiency [10–12, 14–17].

Spiro-OMeTAD is widely used as the hole transporting material (HTM) in perovskite solar cells, even though different HTMs have been successfully used in such devices [18]. It represents a large portion of the cost of the perovskite solar cells, therefore a number of works have focused so far on the possibility to make devices without an HTM [19–21], directly contacting the perovskite with a gold electrode. However, HTM-free devices systematically showed a lower open circuit voltage (V_{oc}) and fill factor (FF) as compared to similar devices with a HTM layer. This has been recently rationalized by Juarez-Perez and co-workers, who demonstrated that a direct contact between the perovskite and the metal electrode enables significant higher recombination losses than the contact between the perovskite and the HTM [22]. However, a metal-perovskite contact could also arise if the perovskite is not homogeneously covered by the HTM layer and this could indeed be an issue for solution processable small molecules [23]. Previous studies in the field of organic electronics have also pointed out the presence of metal migration through the active organic layer during device operation [24–31]. In order to minimize this issue a relatively thick HTM capping layer is needed on the top of the perovskite in solar cells, though this increases the device series resistance which is detrimental for performance [32,33].

Here we demonstrate that electrical shunt pathways in perovskite solar cells, negligible in freshly made devices, become increasingly more important as the device is operated under simulated sun light. We show that a thin layer of Al_2O_3 nanoparticles employed as a buffer layer sandwiched between the perovskite and the HTM inhibits the formation of shunting pathway and meanwhile allowing for a surgical control of the HTM thickness which leads to a substantial gain in the device FF.

In Figure 1 we report the cross sections of perovskite based MSSCs a) as optimized by Ball and co-workers [34] with a 350 nm thick HTM layer and b) with an Al_2O_3 buffer layer between the perovskite and HTM layers. In the same figure we compare the c) J-V characteristics and d) the device performance parameters of these two architectures. Additional data on the forward and backwards scan in the J-V curve, and also the forward and backwards efficiency values in the ageing data are reported in SI.

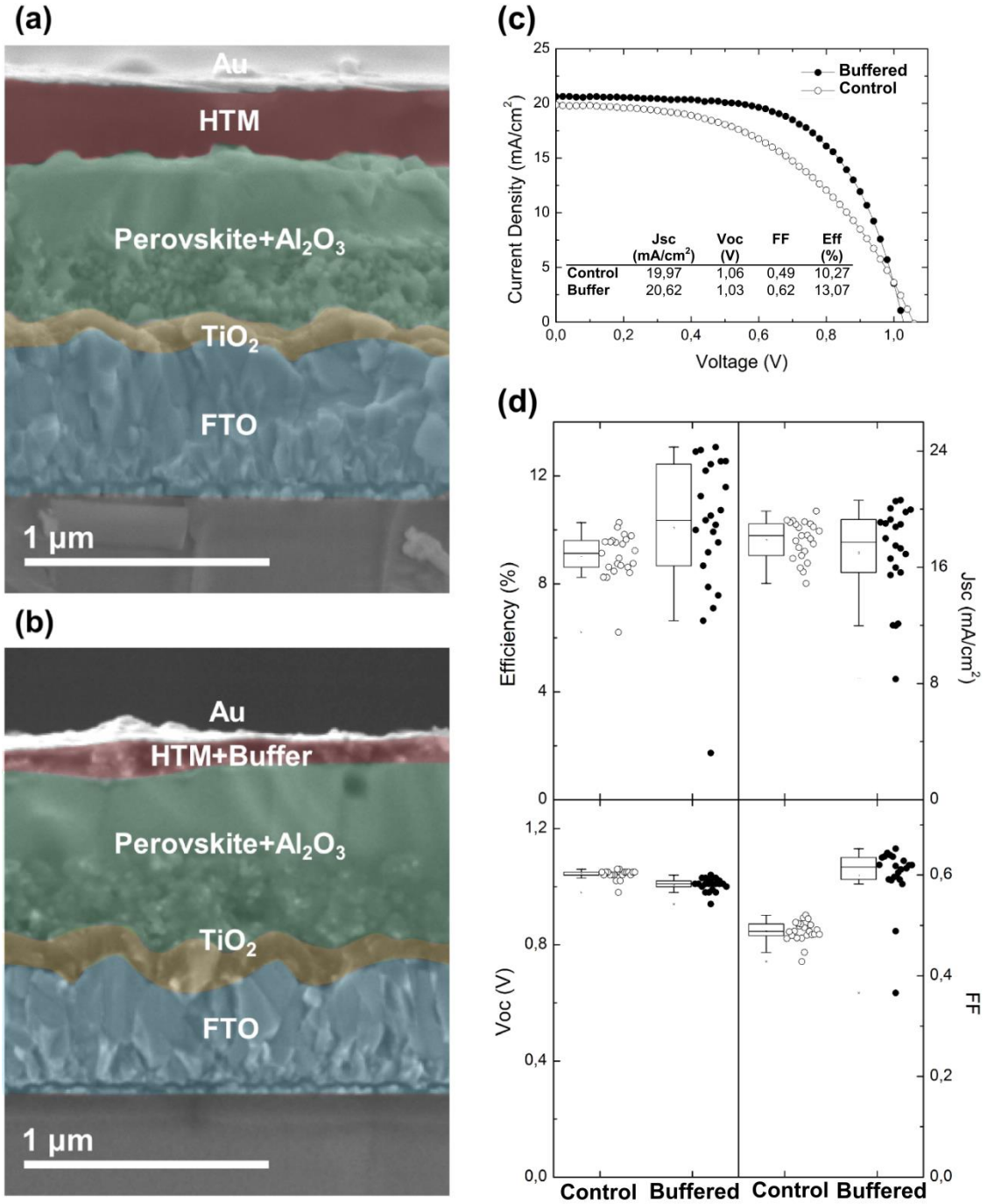

Figure 1. (a) SEM image of a standard MSSC (unbuffered cell); (b) SEM image of a MSSC with a Al_2O_3 buffer layer (buffered cell); (c) J-V curves of the best solar cells realized without (white dots) and with (black dots) a buffer layer; (d) box plot of the device performance parameters of unbuffered cells (white dots) and buffered cells (black dots).

The overall PCEs with Al_2O_3 buffer layers are on average higher than the standard cells without buffer layers. A closer look at the main parameters driving the solar cell performance

shows that the photocurrent generated by the cells does not depend on the device architecture, which suggests that the charge generation and collection is not affected by the presence of the buffer layer. The V_{oc} values are also comparable. The fill factor is the most affected parameter; it is 25% higher in cells with a buffer layer than in standard control cells. Notice that the same trends were observed in 3 different batches of devices (see SI for details).

From the SEM cross-section of the devices (Fig 1a and 1b) it is evident that the presence of the buffer layer allows for a reduction of the HTM layer thickness of about a factor 3. A fresh perovskite cell can be modelled by an equivalent circuit consisting of two diodes [35,36], representing the recombination at each of the device charge selective heterojunctions, in series with two resistors, which represent the resistance associated with the motion of charges through each of the blocking layers (see SI for details). By fitting the dark J-V curves measured from both devices architectures with such a model we found that one factor that contributes to raising the FF in buffered devices is the three times lower series, which is in good agreement with the three times thinner spiro-OMeTAD layer reported in Figure 1 for device with buffer layer.

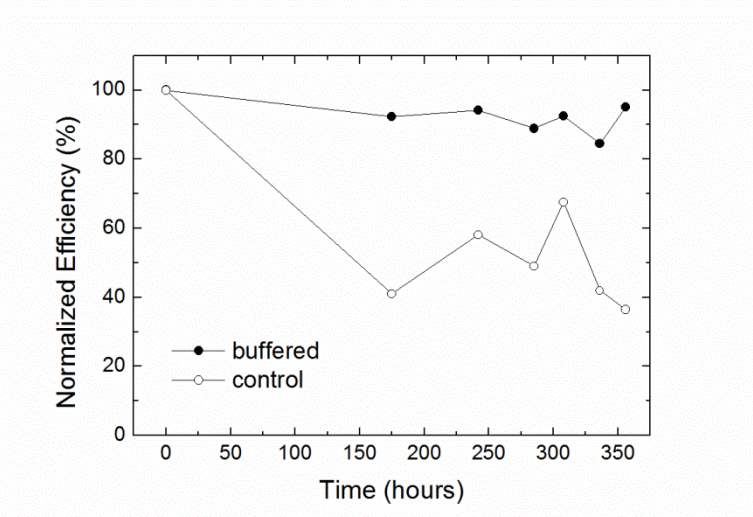

Figure 2. Normalized efficiency of most robust buffered cell (black dots) and unbuffered cell (white dots) under AM1.5G illumination condition.

Assessed the new device architecture we performed an ageing test to check how the buffer layer affects the device performances over time. We left sealed devices under simulated full sunlight (generated from a xenon lamp without UV filtering) up to 350 hours, monitoring the devices performances. We report the PCE as a function of time in Figure 2. Devices without the buffer layer show a rapid deterioration of the performances in the first 200 hours, then they stabilise. The best result we got with a buffered cell shows an efficiency dropping of only 5% after the 350 hour test.

Very similar trends have been observed before for the control devices, without any clear rationalization [37]. So far, moisture has been identified as the major cause of degradation for the hybrid perovskite semiconductor [23,38,39]. However we found no evidence of degradation of the perovskite absorber material after 350 hours under full sun light illumination (see linear absorption spectrum in SI).

Considering the entire device structure, the presence of TiO_2 as hole blocking layer has been found to make the device sensitive to UV radiation [37]. Again, we can exclude this as both device structures studied here present a TiO_2 layer. In the same way we can exclude any phenomena of de-doping of the spiro-OMeTAD due to absence of oxygen since we made use of H-TFSI doping, which allows a stable doping level also in oxygen-free condition [40].

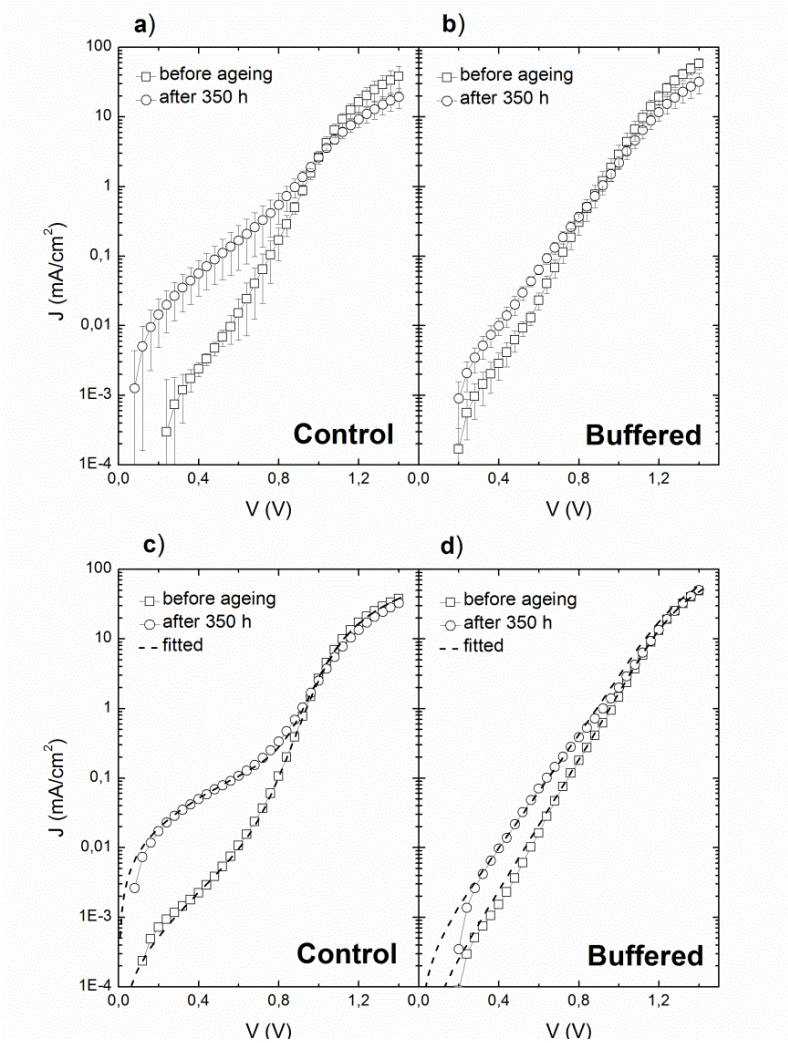

Figure 3. Dark J-V curve before (white squares) and after ageing (white dots) averaged over 4 different devices a) buffered and b) control. Figures c) and d) show the fitting of the dark J-V curve of two of the devices shown in a) and b), a buffered and a control device.

During the ageing test we monitored not only the J-V under illumination, but also the J-V in dark conditions, which we show in Figure 3a for MSSCs with buffer layer and in Figure 3b for standard MSSCs. In these figures, the statistics is obtained from 8 different solar cells, 4 with buffer layer and the other 4 without the buffer layer.

It is well known that in a solar cell the shunting effects become important at low voltages and the series resistance at higher voltages [41]. This means that in presence of a change in the shunting paths of a solar cell, the effect would be clear in the low voltage parts of the J-V

curve. Here, the dark J-V curves of control cells show a clear growth of the current density at low voltages after 350 hours of ageing. On the contrary in cells with the buffer layer the growth of the current at low voltages is reduced. This trend gives a qualitative indication that the shunting pathways form quicker without the buffer layer.

To be more quantitative, we fitted the experimental results (in Figure 3c-d) to a model based on the equivalent circuit shown in SI. This circuit incorporates an additional shunting diode to model the effects of the metal-perovskite contact (see SI for details). By fitting two representative J-V curves showed in Figure 3, one for the control cells and the other for the buffered cells, we extracted that the reverse saturation current density of the shunting diode (I_{shunt}), after device ageing, was two orders of magnitude higher in the control than in the buffered device (see SI). In our model, a higher I_{shunt} indicates a greater proportion of the current flowing through the shunting diode, which is due to metal-perovskite contact. It follows that aged devices without buffer layers suffer from significantly higher shunting losses than those with buff layers. Thus, we conclude that the Al_2O_3 buffer layer protects the perovskite in the presence of pin-holes defects that originate during the deposition of the HTM and/or from electrode migration that could arise under the ageing process. The main consequence of this effect is a considerable improvement of the stability of the power conversion efficiency of devices incorporating the Al_2O_3 mesoporous buffer layer.

In conclusion, we have demonstrated that an important degradation mechanism in perovskite solar cells is activated by a low shunt resistance occurring during aging. We postulate that a direct contact between the metal electrode and the perovskite results in detrimental electronic shunt pathways, which lower the power conversion efficiency. We showed that the occurrence of shunting is negligible in freshly made device, but becomes increasingly more important during the device operation, being responsible for a significant losses in the first few hundreds of hours of operation. In order to minimize this phenomenon, we introduced an insulating buffer layer between the perovskite and the metal contact infiltrating the hole transporter within mesoporous Al_2O_3. The Al_2O_3 buffer layer significantly reduces the shunting degradation, which is consistent with it inhibiting the formation of a direct contact between the metal electrode and the perovskite. This method enabled preparing perovskite devices with nearly no degradation in the first 350 hours under simulated standard full sun light solar illumination. Furthermore, the Al_2O_3 buffer layer allows us to control and reduce the thickness of the hole transporter layer, which results in lower device series resistance and higher power conversion efficiency.

Methods

Device Fabrication. Devices were fabricated on fluorine doped tin oxide (FTO) coated glass substrates. The substrates were cleaned sequentially in Hellmanex, acetone, isopropanol and oxygen plasma. A compact layer of TiO_2 was subsequently deposited via spray pyrolysis at 275°C from a precursor solution of titanium diisopropoxide bis(acetylacetonate) in anhydrous ethanol. The substrate was sintered at 500°C for 45 min and left to cool to room temperature. The samples were then submerged in a 15 mM aqueous $TiCl_4$ bath at 70°C for 1 h, followed by rinsing with deionized water and re-sintering at 500°C for 45 min.

The mesoporous Al_2O_3 scaffold was deposited by spin coating a colloidal dispersion of < 50 nm Al_2O_3 nanoparticles at 20 wt% in isopropanol diluted with isopropanol at a volume ratio of 1:2, at 2000 rpm (ramp: 2000 rpm/s) for 60 s, followed by drying at 150°C for 30 min.

Upon cooling to room temperature, the perovskite layer was deposited in a nitrogen-filled glovebox by spin-coating (speed = 2000 rpm, ramp = 2000 rpm/s, time = 60s) from ~40 wt% dimethylformamide (DMF) solution of methylammonium iodide and $PbCl_2$ (3:1 molar ratio). The substrate was then heated at 100°C for 2 h on a hotplate in the glovebox. A more detailed description of this step has been reported elsewhere [12,34].

Then, a iodopentafluorobenzene (IPFB) solution was used to passivate surface sites as recently reported [42]. The IPFB was deposited in the glovebox by spin-coating (speed = 2000 rpm, ramp = 2000 rpm/s, time = 60s) on top of the perovskite film after the annealing protocol.

Doped 2,2′,7,7′-tetrakis-(N,N-di-pmethoxyphenylamine)9,9′-spirobifluorene (spiro-OMeTAD) solution was prepared just before spin-coating it. We highlight here that the additives composition used to dope the spiro-OMeTAD was different from the traditional lithium bis(trifluoromethanesulfonyl)imide (Li-TFSI) and tert-butylpyridine (tBP). The protic

ionic liquid bis(trifluoromethanesulfonyl)imide (H-TFSI, from Aldrich, CAS Number 82113-65-3) and the inert salt tetraethyl bis-(trifluoromethane)sulfonimide (Et_4N-TFSI, from Aldrich, CAS Number 161401-26-9) were used as doping additives into the spiro-OMeTAD solution. The effect of these two chemicals on the charge transport within the spiro-OMeTAD has been reported elsewhere [40]. The reason of using the new additive composition is mainly because Li-TFSI needs oxygen to effectively dope the spiro-OMeTAD, where H-TFSI can work in an inert atmosphere, such as in nitrogen glovebox condition. A complete comparison between the Li-TFSI and the H-TFSI on the device stability is currently under investigation and will be published elsewhere. To prepare the HTM solution, 80 mM of spiro-OMeTAD solution in chlorobenzene with addition of H-TFSI at a concentration of 1.6 mM was prepared. This solution needs to be thermally activated by leaving the solution in a closed vial overnight at 100°C in inert atmosphere. Finally the Et_4N-TFSI was added after cooling the solution to room temperature with a concentration of 20 mM, before the spin-coating procedure.

In cells with the buffer layer, the concentration of the spiro-OMeTAD and the additives in the CB solvent were halved in order to obtain a thinner capping layer. We underline that all the preparation of the HTM solution was performed without exposing the spiro-OMeTAD and the additives to air and using anhydrous solvents.

The buffer layer was dynamically coated by dropping a colloidal dispersion of < 50 nm Al_2O_3 nanoparticles at 2 wt% in isopropanol directly on to the substrate while spinning at 2000 rpm.

The hole transporter layer was finally deposited in both cases, with and without the buffer layer, by depositing the spiro-OMeTAD solution upon a stationary substrate and then spin-coating at 2000 rpm (ramp: 2000 rpm/s) for 60 s.

Finally, 50 nm of gold was deposited by thermal evaporation under high vacuum to form the cathode.

Device Characterisation. Current-voltage characteristics were measured under AM 1.5 100 $mWcm^{-2}$ simulated sunlight (ABET Technologies Sun 2000) with a Keithley 2400. The apparatus for device characterization was calibrated with an NREL certified KG5 filtered Si reference diode. The solar cells were masked with a metal aperture defining the active area (0.0625 cm^2) of the solar cells. The current-voltage curves were recorded with a sourcemeter (Keithley 2400, USA) scanning at 0.15 V/s from -1.4 to 0 V. Scan-direction dependence of the current-voltage curves[43] are reported in SI.

The long-term ageing measurements were carried out by continuously shining a 100 $mWcm^{-2}$ light (Atlas CPSPlus Xenon lamp) on the devices held at open circuit condition.

Perovskite and Al_2O_3 layers Characterization. Sample thicknesses were measured using a Veeco Dektak 150 surface profilometer. Scanning electron microscopy (SEM) images were obtained using a Hitachi S-4300.

Encapsulation procedure. In order to perform stability tests, the devices were encapsulated in the nitrogen-filled glovebox spreading epoxy resin around the active area to stick a glass slide on the whole device (see the picture in the SI).

ASSOCIATED CONTENT

Supporting Information

Equivalent circuit modelling; a picture of an encapsulated device; additional data for device performances before ageing with and without buffer layer; absorbance spectra of device before and after ageing; statistics of ageing device performance parameters; scan direction dependence of the current voltage curves. This material is available free of charge via the Internet at http://pubs.acs.org.

AUTHOR INFORMATIONS

***Corresponding author**

AA a.abate@epfl.ch, AP annamaria.petrozza@iit.it, HJS h.snaith1@physics.ox.ac.uk

Notes

The authors declare no competing financial interest.

ACKNOWLEDGEMENT

We thank the Engineering and Physical Sciences Research Council (EPSRC) APEX project for financial support and Dr. Ajay Ram Srimath Kandada and Ms. Stefanie Neutzner for useful discussions. J. M. Foster and G. Richardson were part funded by the EPSRC through grant EP/I01702X/.This publication is partially based on work supported by award number KUK-C1-013-04, made by King Abdullah University of Science and Technology (KAUST), via an OCCAM visiting research fellowship awarded to G. Richardson. The project was partially funded by the European Union Seventh Framework Programme [FP7/2007-2013] under grant agreement 316494 and grant agreement n° 604032 of the MESO project.

REFERENCES

(1) Weisz, P. B. Basic Choices and Constraints on Long-Term Energy Supplies. *Phys. Today* **2004**, *57*, 47–52.

(2) Dresselhaus, M. S.; Crabtree, G. W.; Buchanan, M. V. Addressing Grand Energy Challenges through Advanced Materials. *MRS Bull.* **2011**, *30*, 518–524.

(3) Kamat, P. V. Meeting the Clean Energy Demand: Nanostructure Architectures for Solar Energy Conversion. *J. Phys. Chem. C* **2007**, *111*, 2834–2860.

(4) O'Regan, B.; Grätzel, M. A Low-Cost, High-Efficiency Solar Cell Based on Dye-Sensitized Colloidal TiO_2 Films. *Nature* **1991**, *353*, 737–740.

(5) Chiba, Y.; Islam, A.; Watanabe, Y.; Komiya, R.; Koide, N.; Han, L. Dye-Sensitized Solar Cells with Conversion Efficiency of 11.1%. *Jpn. J. Appl. Phys.* **2006**, *45*, L638–L640.

(6) Yella, A.; Lee, H.-W.; Tsao, H. N.; Yi, C.; Chandiran, A. K.; Nazeeruddin, M. K.; Diau, E. W.-G.; Yeh, C.-Y.; Zakeeruddin, S. M.; Grätzel, M. Porphyrin-Sensitized Solar Cells with Cobalt (II/III)-Based Redox Electrolyte Exceed 12 Percent Efficiency. *Science* **2011**, *334*, 629–634.

(7) Bach, U.; Lupo, D.; Comte, P.; Moser, J. E.; Weissortel, F.; Salbeck, J.; Spreitzer, H.; Gratzel, M. Solid-State Dye-Sensitized Mesoporous TiO_2 Solar Cells with High Photon-to-Electron Conversion Efficiencies. *Nature* **1998**, *395*, 583–585.

(8) Cai, N.; Moon, S.-J.; Cevey-Ha, L.; Moehl, T.; Humphry-Baker, R.; Wang, P.; Zakeeruddin, S. M.; Grätzel, M. An Organic D-Π-A Dye for Record Efficiency Solid-State Sensitized Heterojunction Solar Cells. *Nano Lett.* **2011**, *11*, 1452–1456.

(9) Burschka, J.; Dualeh, A.; Kessler, F.; Baranoff, E.; Cevey-Ha, N.-L.; Yi, C.; Nazeeruddin, M. K.; Grätzel, M. Tris(2-(1H-Pyrazol-1-yl)pyridine)cobalt(III) as P-Type Dopant for Organic Semiconductors and Its Application in Highly Efficient Solid-State Dye-Sensitized Solar Cells. *J. Am. Chem. Soc.* **2011**, *133*, 18042–18045.

(10) Zhou, H.; Chen, Q.; Li, G.; Luo, S.; Song, T. -b.; Duan, H.-S.; Hong, Z.; You, J.; Liu, Y.; Yang, Y. Interface Engineering of Highly Efficient Perovskite Solar Cells. *Science (80-.).* **2014**, *345*, 542–546.

(11) Kojima, A.; Teshima, K.; Shirai, Y.; Miyasaka, T. Organometal Halide Perovskites as Visible-Light Sensitizers for Photovoltaic Cells. *J. Am. Chem. Soc.* **2009**, *131*, 6050–6051.

(12) Lee, M. M.; Teuscher, J.; Miyasaka, T.; Murakami, T. N.; Snaith, H. J. Efficient Hybrid Solar Cells Based on Meso-Superstructured Organometal Halide Perovskites. *Science* **2012**, *338*, 643–647.

(13) Noel, N. K.; Abate, A.; Stranks, S. D.; Parrott, E.; Burlakov, V.; Goriely, A.; Snaith, H. J. Enhanced Photoluminescence and Solar Cell Performance via Lewis Base Passivation of Organic-Inorganic Lead Halide Perovskites. *ACS Nano* **2014**, *8*, 9815–9821.

(14) Kim, H.-S.; Lee, C.-R.; Im, J.-H.; Lee, K.-B.; Moehl, T.; Marchioro, A.; Moon, S.-J.; Humphry-Baker, R.; Yum, J.-H.; Moser, J. E.; et al. Lead Iodide Perovskite Sensitized All-Solid-State Submicron Thin Film Mesoscopic Solar Cell with Efficiency Exceeding 9%. *Sci. Rep.* **2012**, *2*, 591.

(15) Heo, J. H.; Im, S. H.; Noh, J. H.; Mandal, T. N.; Lim, C.-S.; Chang, J. A.; Lee, Y. H.; Kim, H.; Sarkar, A.; Nazeeruddin, M. K.; et al. Efficient Inorganic–organic Hybrid Heterojunction Solar Cells Containing Perovskite Compound and Polymeric Hole Conductors. *Nat. Photonics* **2013**, *7*, 486–491.

(16) Burschka, J.; Pellet, N.; Moon, S.-J.; Humphry-Baker, R.; Gao, P.; Nazeeruddin, M. K.; Grätzel, M. Sequential Deposition as a Route to High-Performance Perovskite-Sensitized Solar Cells. *Nature* **2013**, *499*, 316–319.

(17) Jeon, N. J.; Lee, H. G.; Kim, Y. C.; Seo, J.; Noh, J. H.; Lee, J.; Seok, S. Il. O-Methoxy Substituents in Spiro-OMeTAD for Efficient Inorganic-Organic Hybrid Perovskite Solar Cells. *J. Am. Chem. Soc.* **2014**, *136*, 7837–7840.

(18) Abate, A.; Planells, M.; Hollman, D.; Bharti, V.; Chand, S.; Snaith, H.; Robertson, N. Hole-Transport Materials with Greatly-Differing Redox Potentials Give Efficient TiO_2-$[CH_3NH_3][PbX_3]$ Perovskite Solar Cells. *Phys. Chem. Chem. Phys.* **2014**, *17*, 2335–2338.

(19) Etgar, L.; Gao, P.; Xue, Z.; Peng, Q.; Chandiran, A. K.; Liu, B.; Nazeeruddin, M. K.; Grätzel, M. Mesoscopic $CH_3NH_3PbI_3/TiO_2$ Heterojunction Solar Cells. *J. Am. Chem. Soc.* **2012**, *134*, 17396−17399.

(20) Laban, W. A.; Etgar, L. Depleted Hole Conductor-Free Lead Halide Iodide Heterojunction Solar Cells. *Energy Environ. Sci.* **2013**, *6*, 3249.

(21) Shi, J.; Dong, J.; Lv, S.; Xu, Y.; Zhu, L.; Xiao, J.; Xu, X.; Wu, H.; Li, D.; Luo, Y.; et al. Hole-Conductor-Free Perovskite Organic Lead Iodide Heterojunction Thin-Film Solar Cells: High Efficiency and Junction Property. *Appl. Phys. Lett.* **2014**, *104*, 063901.

(22) Juarez-Perez, E. J.; Wuβler, M.; Fabregat-Santiago, F.; Lakus-Wollny, K.; Mankel, E.; Mayer, T.; Jaegermann, W.; Mora-Sero, I. Role of the Selective Contacts in the Performance of Lead Halide Perovskite Solar Cells. *J. Phys. Chem. Lett.* **2014**, *5*, 680–685.

(23) Eperon, G. E.; Burlakov, V. M.; Docampo, P.; Goriely, A.; Snaith, H. J. Morphological Control for High Performance, Solution-Processed Planar Heterojunction Perovskite Solar Cells. *Adv. Funct. Mater.* **2014**, *24*, 151–157.

(24) Grossiord, N.; Kroon, J. M.; Andriessen, R.; Blom, P. W. M. Degradation Mechanisms in Organic Photovoltaic Devices. *Org. Electron.* **2012**, *13*, 432–456.

(25) Rösch, R.; Tanenbaum, D. M.; Jørgensen, M.; Seeland, M.; Bärenklau, M.; Hermenau, M.; Voroshazi, E.; Lloyd, M. T.; Galagan, Y.; Zimmermann, B.; et al. Investigation of the Degradation Mechanisms of a Variety of Organic Photovoltaic Devices by Combination of Imaging Techniques—the ISOS-3 Inter-Laboratory Collaboration. *Energy Environ. Sci.* **2012**, *5*, 6521.

(26) Song, W.; Li, Z.; So, S. K.; Qiu, Y.; Zhu, Y.; Cao, L. Dynamic SIMS Characterization of Interface Structure of Ag/Alq3/NPB/ITO Model Devices. *Surf. Interface Anal.* **2001**, *32*, 102–105.

(27) Song, W.; So, S. K.; Moulder, J.; Qiu, Y.; Zhu, Y.; Cao, L. Study on the Interaction between Ag and tris(8-Hydroxyquinoline) Aluminum Using X-Ray Photoelectron Spectroscopy. *Surf. Interface Anal.* **2001**, *32*, 70–73.

(28) Grandin, H. M.; Tadayyon, S. M.; Lennard, W. N.; Griffiths, K.; Coatsworth, L. L.; Norton, P. R.; Popovic, Z. D.; Aziz, H.; Hu, N. X. Rutherford Backscattering and Secondary Ion Mass Spectrometry Investigation of Mg:Ag–tris(8-Hydroxy Quinoline) Aluminum Interfaces. *Org. Electron.* **2003**, *4*, 9–14.

(29) Docampo, P.; Snaith, H. J. Obviating the Requirement for Oxygen in SnO_2-Based Solid-State Dye-Sensitized Solar Cells. *Nanotechnology* **2011**, *22*, 225403.

(30) Pathak, S. K.; Abate, A.; Leijtens, T.; Hollman, D. J.; Teuscher, J.; Pazos, L.; Docampo, P.; Steiner, U.; Snaith, H. J. Towards Long-Term Photostability of Solid-State Dye Sensitized Solar Cells. *Adv. Energy Mater.* **2014**, *4*, 1301667–1301667.

(31) Roesch, R.; Eberhardt, K.-R.; Engmann, S.; Gobsch, G.; Hoppe, H. Polymer Solar Cells with Enhanced Lifetime by Improved Electrode Stability and Sealing. *Sol. Energy Mater. Sol. Cells* **2013**, *117*, 59–66.

(32) Ding, I.-K.; Tétreault, N.; Brillet, J.; Hardin, B. E.; Smith, E. H.; Rosenthal, S. J.; Sauvage, F.; Grätzel, M.; McGehee, M. D. Pore-Filling of Spiro-OMeTAD in Solid-State Dye Sensitized Solar Cells: Quantification, Mechanism, and Consequences for Device Performance. *Adv. Funct. Mater.* **2009**, *19*, 2431–2436.

(33) Dualeh, A.; Moehl, T.; Tétreault, N.; Teuscher, J.; Gao, P.; Nazeeruddin, M. K.; Grätzel, M. Impedance Spectroscopic Analysis of Lead Iodide Perovskite-Sensitized Solid-State Solar Cells. *ACS Nano* **2014**, *8*, 362–373.

(34) Ball, J. M.; Lee, M. M.; Hey, A.; Snaith, H. J. Low-Temperature Processed Meso-Superstructured to Thin-Film Perovskite Solar Cells. *Energy Environ. Sci.* **2013**, *6*, 1739.

(35) Foster, J. M.; Snaith, H. J.; Leijtens, T.; Richardson, G. A Model for the Operation of Perovskite Based Hybrid Solar Cells: Formulation, Analysis and Comparison to Experiment. *to Appear SIAM J. Appl. Math.* **2014**.

(36) Ishaque, K.; Salam, Z.; Taheri, H. Simple, Fast and Accurate Two-Diode Model for Photovoltaic Modules. *Sol. Energy Mater. Sol. Cells* **2011**, *95*, 586–594.

(37) Leijtens, T.; Eperon, G. E.; Pathak, S.; Abate, A.; Lee, M. M.; Snaith, H. J. Overcoming Ultraviolet Light Instability of Sensitized TiO_2 with Meso-Superstructured Organometal Tri-Halide Perovskite Solar Cells. *Nat. Commun.* **2013**, *4*, 2885.

(38) Noh, J. H.; Im, S. H.; Heo, J. H.; Mandal, T. N.; Seok, S. Il. Chemical Management for Colorful, Efficient, and Stable Inorganic-Organic Hybrid Nanostructured Solar Cells. *Nano Lett.* **2013**, *13*, 1764–1769.

(39) Suarez, B.; Gonzalez-Pedro, V.; Ripolles, T. S.; Sanchez, R. S.; Otero, L.; Mora-Sero, I. Recombination Study of Combined Halides (Cl, Br, I) Perovskite Solar Cells. *J. Phys. Chem. Lett.* **2014**, *5*, 1628–1635.

(40) Abate, A.; Hollman, D. J.; Teuscher, J.; Pathak, S.; Avolio, R.; D'Errico, G.; Vitiello, G.; Fantacci, S.; Snaith, H. J. Protic Ionic Liquids as P-Dopant for Organic Hole Transporting Materials and Their Application in High Efficiency Hybrid Solar Cells. *J. Am. Chem. Soc.* **2013**, *135*, 13538–13548.

(41) Foster, J. M.; Kirkpatrick, J.; Richardson, G. Asymptotic and Numerical Prediction of Current-Voltage Curves for an Organic Bilayer Solar Cell under Varying Illumination and Comparison to the Shockley Equivalent Circuit. *J. Appl. Phys.* **2013**, *114*, 104501.

(42) Abate, A.; Saliba, M.; Hollman, D. J.; Stranks, S. D.; Wojciechowski, K.; Avolio, R.; Grancini, G.; Petrozza, A.; Snaith, H. J. Supramolecular Halogen Bond Passivation of Organic-Inorganic Halide Perovskite Solar Cells. *Nano Lett.* **2014**, *14*, 3247–3254.

(43) Snaith, H. J.; Abate, A.; Ball, J. M.; Eperon, G. E.; Leijtens, T.; Noel, N. K.; Stranks, S. D.; Wang, J. T.; Wojciechowski, K.; Zhang, W. Anomalous Hysteresis in Perovskite Solar Cells. *J. Phys. Chem. Lett.* **2014**, *5*, 1511–1515.